Optical Coherence Tomography as a Rapid, Accurate, Noncontact Method of Visualizing the Palisades of Vogt

Kira L. Lathrop,[1] *Divya Gupta,*[1] *Larry Kagemann,*[1,2] *Joel S. Schuman,*[1,2,3] *and Nirmala SundarRaj*[1,3,4]

Purpose. This study explored the efficacy of optical coherence tomography (OCT) as a high-resolution, noncontact method for imaging the palisades of Vogt by correlating OCT and confocal microscopy images.

Methods. Human limbal rims were acquired and imaged with OCT and confocal microscopy. The area of the epithelial basement membrane in each of these sets was digitally reconstructed, and the models were compared.

Results. OCT identified the palisades within the limbus and exhibited excellent structural correlation with immunostained tissue imaged by confocal microscopy.

Conclusions. OCT successfully identified the limbal palisades of Vogt that constitute the corneal epithelial stem cell niche. These findings offer the exciting potential to characterize the architecture of the palisades in vivo, to harvest stem cells for transplantation more accurately, to track palisade structure for better diagnosis, follow-up and staging of treatment, and to assess and intervene in the progression of stem cell depletion by monitoring changes in the structure of the palisades. (*Invest Ophthalmol Vis Sci.* 2012;53:1381–1387) DOI:10.1167/iovs.11-8524

The palisades of Vogt were first noted in the corneoscleral limbus in 1866 and were described in detail in 1921,[1] but to date they are not well defined or understood. Recent progress in stem cell research has focused attention on the palisades as the location of the stem cells that maintain corneal epithelial homeostasis and clarity.[2–7] Ideally, the corneal stem cells would be visualized directly; however, in the absence of such technology, the palisades can be used to determine the general location and status of the stem cells. Defining the palisades has proven challenging because of their unique structure, configuration, and dimension in each person and because they are difficult to visualize. The limbal palisades provide a crucial environment for the maintenance of epithelial stem cells. Understanding the palisades is necessary for developing new stem cell therapies targeted at restoring vision and maintaining the health of the eye.[8] The convergence of progress in the development of optical coherence tomography (OCT), advances in three-dimensional (3D) stitching and rendering techniques, and improvements in immunofluorescence staining and microscopy now offers the opportunity to reexamine the structure of the palisades in general and to visualize the full structure of the palisades in vivo for the first time.

Residing in a 1- to 2-mm band of the connective tissue primarily in the superior and inferior regions of the corneoscleral limbus, the palisades have a structure as unique as fingerprints.[2,8] The size, shape, and configuration of the palisades change over time and in response to acquired or congenital conditions, aging, surgery, and medication.[1,3,4,7,9–19] Destruction of the palisades and the associated destruction of the stem cells they contain results in conjunctivalization of the cornea, vascular invasion, and concomitant blindness. When the palisades and their resident stem cells are replaced before stromal scarring, normal corneal epithelium can be reestablished and vision restored. Once scarring occurs, a corneal transplant is also required.[3,20]

Visualization of portions of the palisades is sometimes possible using a slit lamp and can be enhanced by fluorescein imaging.[2] However, in up to 20% of patients, the palisades cannot be identified clinically using current methods,[1,9,21] and none of these techniques give an overall view of the dimension and structure of the whole palisades region. Recently, in vivo confocal microscopy has been used to visualize the palisades and has been proposed as a technique to monitor the status of keratolimbal allografts after transplantation, but the technique is limited by high magnification that restricts the area of the scan.[7–9,21] In addition, in vivo confocal microscopy requires direct contact with the eye and anesthesia, either of which may inadvertently cause more damage to an eye that has already undergone insult. OCT offers an alternative imaging modality that eliminates all these limitations. Here we establish that OCT is capable of high-resolution, noncontact imaging of the palisades of Vogt.

Methods

Twenty human donor corneal rims were recovered in organ culture chambers containing storage medium (Optisol GS; Baush & Lomb, Rochester, NY), as provided by the tissue bank after corneal transplant surgery. Tissue was from donors 24 to 70 years of age and was fixed 2 to 7 days postmortem. Epithelium had been removed around the corneal button during the surgery but was present in the limbal region and conjunctiva.

OCT imaging of human corneal rims was performed with a prototype system that has been previously described.[22] Rims were imaged with a hsUHR-OCT scanner using a raster pattern. Scans sampled a 2 × 2 × 2-mm region of tissue with 512 × 180 × 1024 measurements. The

From the [1]Department of Ophthalmology, UPMC Eye Center, Eye and Ear Institute, Ophthalmology and Visual Science Research Center, and the [3]McGowan Institute for Regenerative Medicine, University of Pittsburgh School of Medicine, Pittsburgh, Pennsylvania; and the [2]Department of Bioengineering, Swanson School of Engineering, and the [4]Department of Cell Biology and Physiology, University of Pittsburgh, Pittsburgh, Pennsylvania.

Supported by National Institutes of Health Core Grant for Vision Research EY08090 and Grant EY03263 (NSR), the Western Pennsylvania Medical Eye Bank (KLL), the Eye and Ear Foundation of Pittsburgh, and Research to Prevent Blindness.

Submitted for publication September 2, 2011; revised November 17, 2011; accepted January 11, 2012.

Disclosure: **K.L. Lathrop**, P; **D. Gupta**, None; **L. Kagemann**, P; **J.S. Schuman**, Carl Zeiss Meditec (I), P; **N. SundarRaj**, None

Corresponding author: Kira L. Lathrop, University of Pittsburgh School of Medicine, Department of Ophthalmology, Eye and Ear Institute, Room 1026, 203 Lothrop Street, Pittsburgh, PA 15213; lathropkl@upmc.edu.

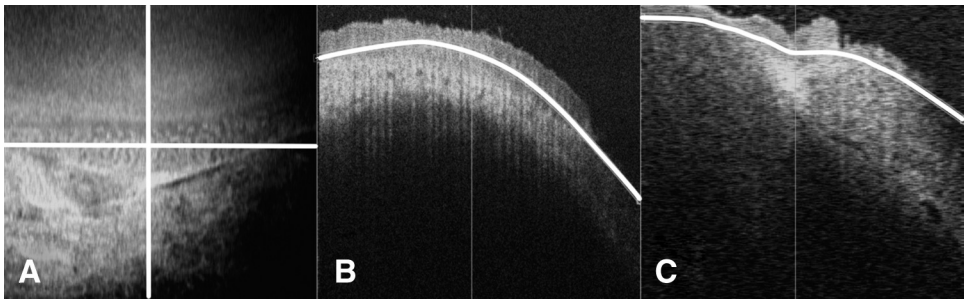

FIGURE 1. C-mode imaging allows sectioning along any plane to view a tissue. Depth can be adjusted to accommodate the depth of the tissue. (**A**) En face image with horizontal and vertical axes of orthogonal sections marked. (**B**) Horizontal orthogonal view showing the planes that are included in the en face image in *white*. (**C**) Vertical view showing the planes that are included in the en face view in *white*.

scanner was custom built with a 100-nm bandwidth light source centered at 870 nm and yielding a coherence length of 2 μm in tissue. Images were reconstructed and processed using SOCT browser software developed by Hiroshi Ishikawa (University of Pittsburgh), MetaMorph (Molecular Devices) and FIJI (ImageJ software [developed by Wayne Rasband, National Institutes of Health, Bethesda, MD; available at http://rsb.info.nih.gov/ij/index.html]) software.

Immunolabeling was performed by washing the corneal rims with phosphate-buffered saline (PBS) for 15 minutes twice before fixation in 4% paraformaldehyde overnight at 4°C. The following day the tissue was washed in PBS-Tx (PBS containing 0.3% Triton X-100) for 15 minutes three times and then permeabilized with 0.5% Triton X-100 for 2 hours at room temperature (RT). After permeabilization, the tissue was washed with PBS-Tx for 5 minutes three times. Blocking was performed by using 10% heat-inactivated goat serum (containing 0.3% Triton X-100) for 2 hours at RT. Tissue was then washed with PBS-Tx for 10 minutes at RT and incubated with culture supernatants containing primary mouse monoclonal anti–human type VII collagen antibody 5D2 (from SundarRaj, University of Pittsburgh, Pittsburgh, PA) diluted 1:1 with the blocking buffer at RT for 1 hour, followed by incubation at 4°C overnight. The tissue was then washed with PBS-Tx for 20 minutes 5 times. Alexa-Fluor 488–conjugated goat anti–mouse IgG was used for the secondary antibody and was incubated for 2 hours at RT in the dark. DAPI (50 μL, 300 nM) was added directly on the secondary antibody for 20 minutes. Finally, the tissue was washed with PBS-Tx for 20 minutes three times and was mounted (Immu-mount; Thermo-electron Incorporated, Pittsburgh, PA). Large-format spacers for whole mounting human corneal rims were made from shelf liner (Duck; ShurTech Brands, Avon, OH). One-inch circles were punched with a lever punch (Fiskars, Helsinki, Finland), and the spacer was fixed to a large format slide (Gorilla Glue, Cincinnati, OH). Corneal rims were cut in half, and relief cuts were made in the sclera and cornea to allow the rim to lie flat. The corneal rims were placed in the well created by the spacer and mounting medium (Immu-mount; Thermo-electron Incorporated) was used to fill the well. Large-format coverslips were used to seal the mounted specimens. Whole mounting the tissue with spacers offers the distinct advantage of maintaining the morphology of the tissue, which is critical for accurate 3D reconstruction.

Confocal microscopy was conducted on an inverted laser scanning confocal microscope system (FV1000; Olympus, Tokyo, Japan) with a 20× oil (refractive index 0.85) objective. Image stack acquisition was undersampled in the XY plane and optimized for the Z dimension to allow the best possible reconstructions and to control file sizes and acquisition time. The depth of the stacks ranged from 50 to 150 μm. Images were saved in the native OIB format and subsequently converted to 8-bit RGB with imaging software (MetaMorph; Molecular Devices, Sunnyvale, CA).

Reference image sets of corneal rims whole mounted and immunofluorescently labeled to define the basement membrane of the limbus were acquired with laser scanning confocal microscopy. Large (up to 50) sequential confocal stack sets were stitched together in FIJI with the 2D/3D plug-in,[23] and 3D models were built using the 3D Viewer plug-in.[24] This kind of acquisition and reconstruction is not possible in living subjects because of the need for a fluorescent label and the time required for acquisition. 3D display of reconstructed stacks is available as Supplementary Movies S1–S4 (http://www.iovs.org/lookup/suppl/doi:10.1167/iovs.11-8524/-/DCSupplemental). OCT image sets were reconstructed in the SOCT browser, smoothed with a rolling average, and viewed in a selective en face mode using C-mode slicing.[25] The

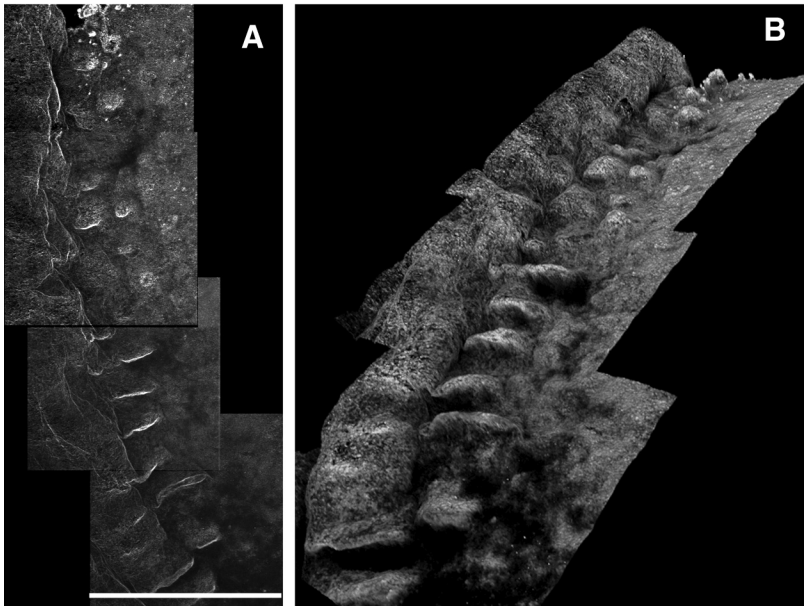

FIGURE 2. Serial confocal stacks labeled with collagen VII stitched and reconstructed in 3D. (**A**) Maximum intensity projection through z-plane reveals overall limbal structure. Scale bar, 635 μm. (**B**) The same stack reconstructed in 3D and rotated to show the orientation of structures relative to each other.

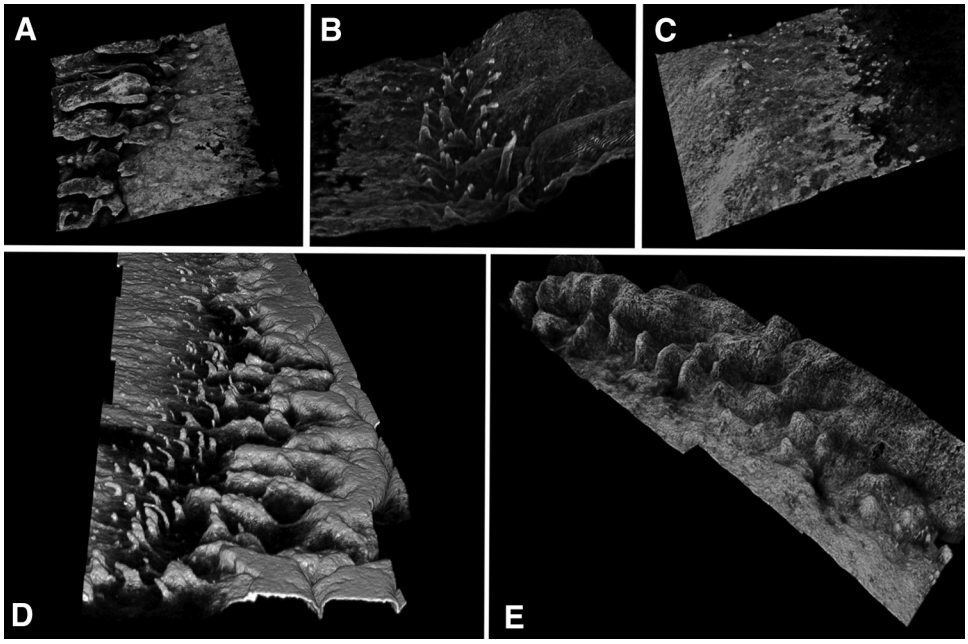

FIGURE 3. (**A–C**) 3D confocal reconstructions of different areas of the limbus from the same subject (see Supplementary Movies S1–S3, http://www.iovs.org/lookup/suppl/doi:10.1167/iovs.11-8524/-/DCSupplemental). (**D**) 3D reconstruction of a limbal region showing an extensive finger-like pattern. (**E**) 3D reconstruction of a limbal region showing an undulating and irregular palisade pattern.

confocal and OCT image sets were correlated to identify the same palisade structures.

RESULTS

In some instances the epithelium had been damaged or removed; however, the specificity of the basement membrane label allowed identification of the limbal region. We were unable to image the full palisades region in approximately one-third of the rims because the anterior portion of the palisades extended all the way to the cut edge of the cornea. Even though some structure could be visualized, these rims were not included for correlation because they might not have provided a true representation of the morphology. Anatomic orientation of the tissue was not available with limbal rims, but, consistent with previous reports,[1] we often found areas of palisades directly across from each other that were presumed to represent superior and inferior positions in the rims. In some instances, the palisades were present almost all the way around the cornea, and this configuration has also been reported.[15] The pattern of the palisades varied within each sample.

OCT image sets were acquired before or after tissue fixation with no significant difference in image quality. Initial reconstruction and processing in SOCT browser software included a rolling average to smooth the image. En face imaging was sometimes able to hint at the underlying structure, but it was inadequate for a full understanding of the region. Detailed visualization of the palisades region was conducted with C-mode sectioning, which allows data to be sectioned virtually along arbitrary planes and in varying thicknesses relative to the direction of scan acquisition. This allows structures embedded within a volume to be exposed and improves the visualization of pathologic features (Fig. 1).[25,26]

This method of mounting the tissue for laser scanning confocal microscopy allowed the acquisition of many contiguous stacks of large areas of tissue without distorting the morphology. These stacks were stitched together to enable viewing of a large area of the limbus; the reconstructions revealed detailed 3D structure of the palisades that has not previously been well represented (Fig. 2). In addition to presenting the variability of the palisade structures, these images reveal the dimension and variability of the limbal structure and the transition of the limbus to the cornea and conjunctiva.

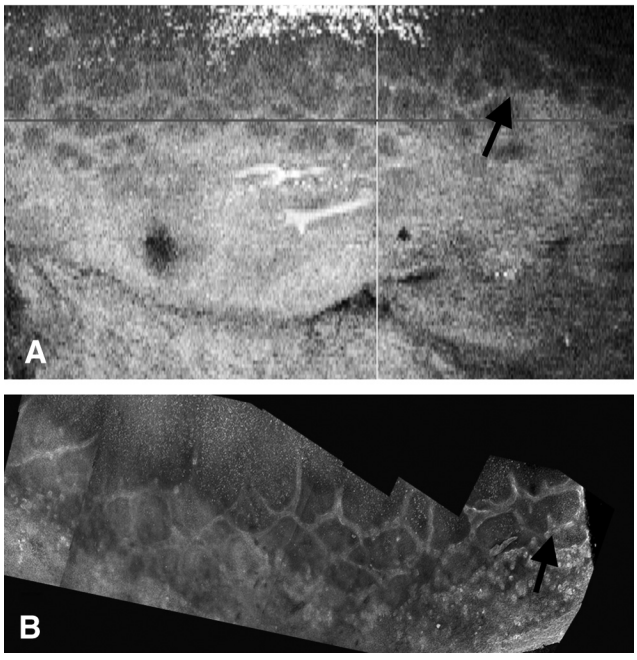

FIGURE 4. Correlation of unmounted OCT and confocal images. (**A**) Unmounted tissue reconstructed in C-mode imaging showing a mesh-like palisades pattern. (**B**) The same region reconstructed with confocal stacks stitched together. There is a slight change in the angle between the two images because the region was flatter for confocal imaging. The *black arrows* identify an easily recognizable structure, but the whole meshwork can be identified in each image.

When the confocal stacks are reconstructed in 3D or rendered with maximum intensity projections through the stack, they reveal a complex and varied structure that demonstrates a wide range of different configurations even within the same subject (Fig. 3). All the observed structures arise from the basement membrane into the epithelium when viewed in 3D. Often ridgelike areas taper off to fingerlike projections in lateral and central areas, giving the impression that the fingerlike regions are the beginning or end of the ridges. These structures have been previously described as focal stromal projections.[8] In some areas the ridges are meshlike whereas in other areas they are clear and rhythmic, with some showing many fingerlike structures. In some samples, there are very few palisade ridges or just a few of the fingerlike structures.

OCT and confocal image stacks were then compared to identify the same regions in each imaging method. The correlation between the methods is clear whether OCT is acquired in unfixed or fixed and mounted tissue (Figs. 4, 5). Reconstruction in 3D reinforces the correlation between the two methods and clearly demonstrates the ability of OCT to reveal detailed and intricate structures in the limbus (Fig. 6). These same image sets can be reconstructed into 3D volumetric models that provide more information about the depth of the palisades and their relationship to each other (Fig. 7).

Volumetric data sets provide more information about the limbus than has previously been available. The overall pattern of the palisades can be viewed (Fig. 8) and the zoom level increased to provide a more restricted field with greater detail. Reviewing of volume data sets can also provide information about how tissue is handled and the integrity of different tissue layers. In some instances, reconstruction revealed palisades areas that extended all the way to the cut edge of the cornea (Fig. 9).

Discussion

Direct visualization of corneal epithelial stem cells in vitro is not possible, but because the palisades provide the environment necessary for the survival of these cells, they can be used as a general indicator of the overall health of the limbus and the presence of stem cells. Townsend[1] reported three distinct palisades patterns in 1991: a standard pattern, an exaggerated pattern, and an attenuated pattern. The patterns we observed fall generally into these three categories, but it is likely that further characterization of the palisade structures may produce finer distinctions in both types and overall dimensions of the structures. This study and others[27,28] clearly illustrate the need to develop a deeper understanding of the architecture of the palisades and to define the relationship of that structure to a functional stem cell population. Here, the rapid acquisition of images with OCT allowed acquisition of 3D volumes that encompass large areas of the limbus, providing image sets that can be acquired from living patients, and are not available with other imaging technologies. Other imaging methods have distinct limitations when working with a structure as dynamic as the limbus. They cannot describe the overall structure of the palisades and cannot effectively evaluate changes in the pali-

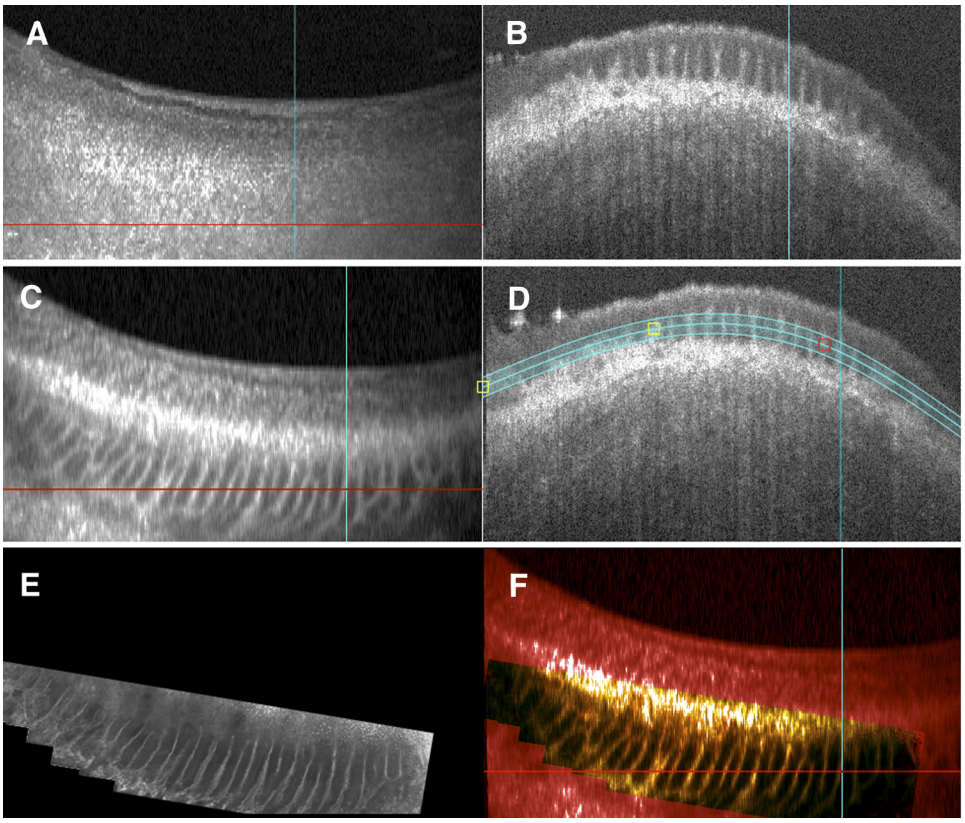

Figure 5. Correlation of mounted OCT tissue and confocal images. (**A**) En face view of tissue. (**B**) Orthogonal view of tissue at the level of the *red line*. (**C**) En face C-mode image reconstructed through the palisades region. (**D**) Orthogonal view of C showing the planes included in the reconstruction. (**E**) Maximum intensity projection of a series of 48 confocal image stacks stitched together to show the same region of the limbus. (**F**) Overlay of OCT en face C-mode image (*red*) and the confocal maximum intensity stitched image (*green*). Coincident areas display in *yellow*. There is no distortion between these image sets because they were both acquired from the same mounted tissue.

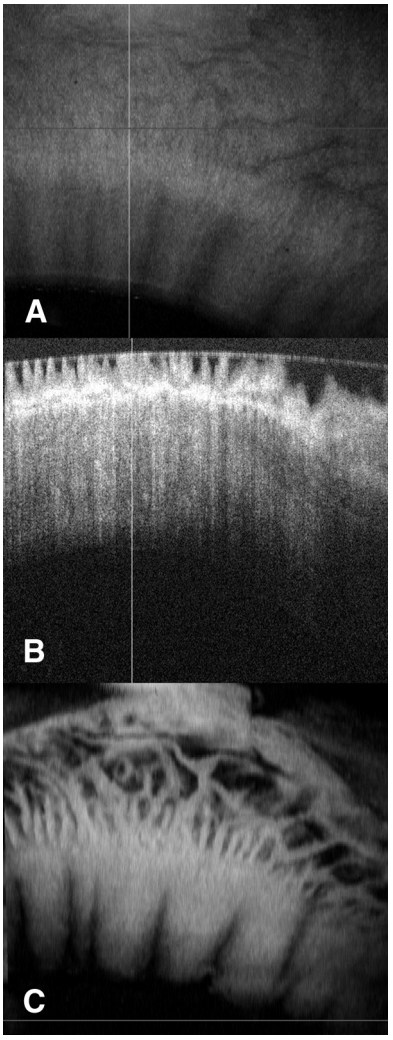

FIGURE 6. Example of extensive detail available in OCT with C-mode reconstruction. (**A**) En face image of limbal rim. (**B**) Orthogonal view showing palisade structures. (**C**) C-mode reconstruction of palisades region showing a regular palisades pattern in the anterior limbus with an extensive meshwork pattern in the posterior limbus.

sades over time. Observation and classification of overall palisades patterns requires these macroscopic views, and the convenience and speed of OCT imaging makes clinical recording and tracking of palisade structure possible for the first time.

Image sets acquired with OCT and reconstructed with C-mode imaging in the present study provided a complex, detailed representation of this unique structure and revealed it to be more intricate than previously described. Similarly, 3D reconstructions from laser scanning confocal imaging also provided a detailed and complex portrait of this perplexing region and underscored the necessity of 3D visualization of the palisades and the need for further understanding of the structure, function, and interactions therein. Areas with distinct, clear structures could be matched between the two imaging modalities to demonstrate that OCT does image the palisades. However, the posterior palisades area was sometimes convoluted and in some instances extended more deeply than confocal microscopy could penetrate. In these areas, OCT was able to provide a more accurate representation of the palisade structure (Figs. 6, 8), and the folding was complex. Orthogonal images similar to those shown by Dua et al.[29] could be found, but it is not yet clear whether true crypts are depicted or whether these shapes are created by the intricate folds.

The noncontact nature and speed of OCT imaging could greatly facilitate future studies of the palisades of Vogt. These investigations can reveal details of the anatomic status and changes in the limbus and allow us to correlate those changes with different disease processes, with postsurgical remodeling and restoration of the palisades and in normal aging. Investigation into the palisade structure present in children and young adults could allow us to understand developmental changes in the palisades. OCT imaging has the potential to enable researchers to interpret the significance of the palisade structure in relation to different conditions and to determine the impact of variations in the size and pattern of palisades on corneal physiology. In the clinic, visualization of the full di-

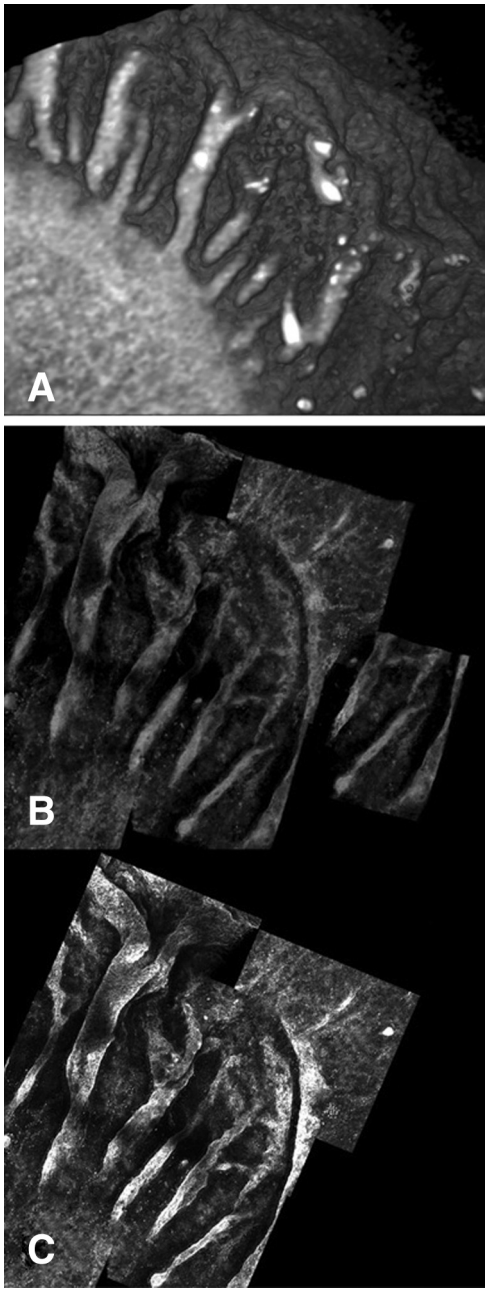

FIGURE 7. (**A**) 3D reconstruction of OCT image set showing palisades pattern (**B**) 3D reconstruction of confocal microscopy stack set showing the same region. (**C**) Maximum intensity projection of the area shown in (**B**) (see Supplementary Movie S4, http://www.iovs.org/lookup/suppl/doi:10.1167/iovs.11-8524/-/DCSupplemental).

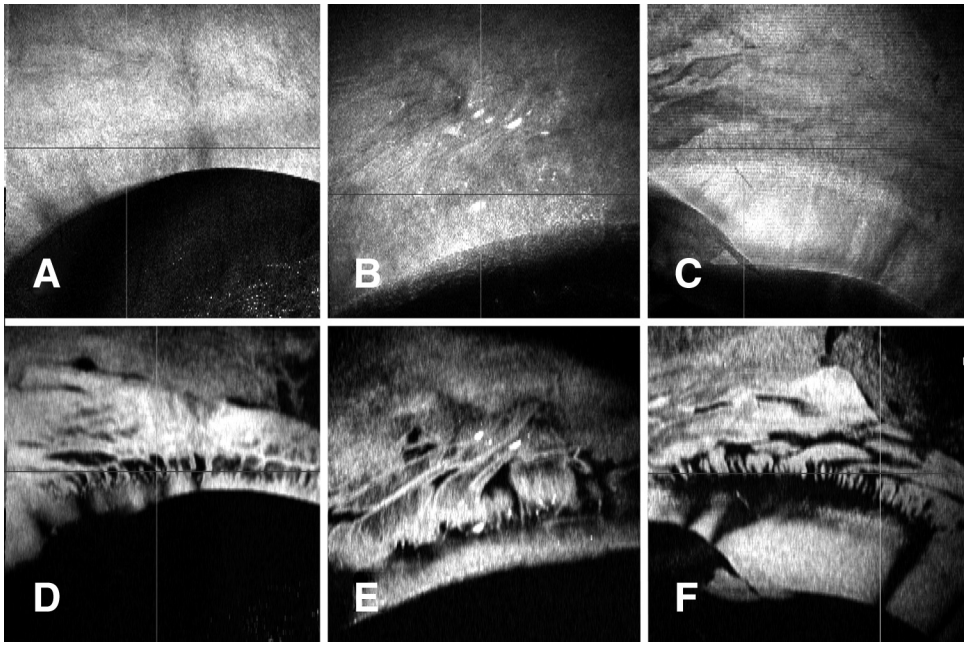

FIGURE 8. Examples of different palisades patterns revealed by OCT. (**A–C**) En face views of the surface of the tissue. (**D–F**) C-mode views of the corresponding palisades regions showing a wide variety of palisades patterns.

mension of the palisades of individual patients could allow temporal tracking of changes in the palisades. Evaluation of the entire corneal stem cell niche of a donor eye before harvesting for autograft would allow better harvesting and enhance targeted biopsies, as described by Shortt et al.,[8] and would help to ensure the health of the donor eye. For patients with full limbal stem cell deficiency, this might allow the success of the limbal transplant to be assessed before corneal transplantation. After corneal surgery, OCT evaluation of the palisades could provide an opportunity to preemptively diagnose and intervene to treat transplants in danger of failure. Further investigation into the distinctions between different palisades configurations could reveal remodeling patterns in the palisades that are indicative of different conditions, and this could potentially become an early diagnostic tool. The image processing used in this study to view selective en face fields of the limbus was conducted after processing, and, though this is acceptable for research, development of analysis tools and software that allow real-time selective en face reconstruction of this specific region will make OCT an even more valuable clinical and surgical tool.

During imaging studies, we observed that many of the limbal rims available after transplantation were not useful for full reconstruction and description of the 3D morphology because the anterior palisades region had been clipped during harvesting of the corneal button. This could simply have resulted from handling during punching of the button and processing before surgery, or the button might have been rejected for transplantation after punching. However, it is possible that the unintentional transplantation of small anterior portions of the limbal palisades has an effect on the postsurgical success of corneal transplants; this possibility bears further investigation.

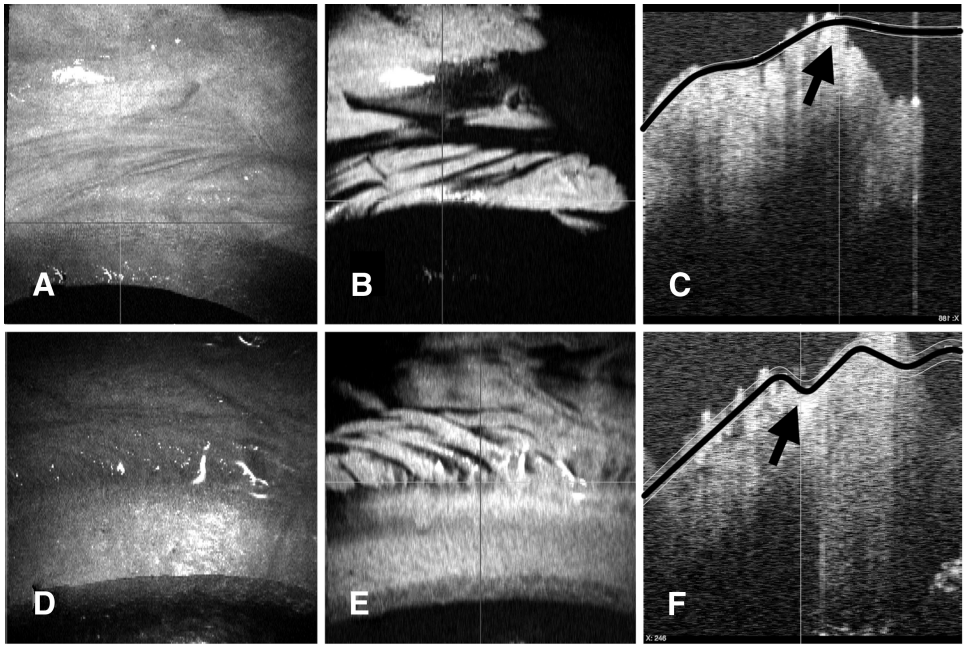

FIGURE 9. Example of possible areas of clipped palisades. (**A**, **D**) The en face view shows the cut edge that is not perpendicular to the surface of the cornea. From this angle it does not appear that there has been any clipping. (**B**, **E**) C-mode reconstructions at the level of the palisades showing palisade structures coming right up to, and ending abruptly at, the cut edge. (**C**, **F**) Vertical orthogonal views of the same section showing the cut edge of the cornea. The planes of the C-mode display are marked in *black*, and the area of the cut edge is highlighted with a *black arrow*. These cuts are stepped in two stages.

In summary, OCT is able to safely and effectively image the palisades of Vogt. This capability has the potential to enhance our understanding of this stem cell niche, allow development of new clinical and research techniques, and assist in developing a better understanding of the scope and function of the corneal epithelial stem cell niche.

Acknowledgments

The authors thank Robert L. Hendricks for consultation and manuscript review, James Funderburgh for consultation, and Hiroshi Ishikawa for developing the SOCT software.

References

1. Townsend WM. The limbal palisades of Vogt. *Trans Am Ophthalmol Soc.* 1991;89:721–56:721–756.
2. Goldberg MF, Bron AJ. Limbal palisades of Vogt. *Trans Am Ophthalmol Soc.* 1982;80:155–71:155–171.
3. Echevarria TJ, Di Girolamo N. Tissue-regenerating, vision-restoring corneal epithelial stem cells. *Stem Cell Rev.* 2011;7:256–268.
4. Kinoshita S, Adachi W, Sotozono C, et al. Characteristics of the human ocular surface epithelium. *Prog Retin Eye Res.* 2001;20:639–673.
5. Wolosin JM, Budak MT, Akinci MA. Ocular surface epithelial and stem cell development. *Int J Dev Biol.* 2004;48:981–991.
6. Budak MT, Alpdogan OS, Zhou M, Lavker RM, Akinci MA, Wolosin JM. Ocular surface epithelia contain ABCG2-dependent side population cells exhibiting features associated with stem cells. *J Cell Sci.* 2005;118(pt 8):1715–1724.
7. Hong J, Zheng T, Xu J, et al. Assessment of limbus and central cornea in patients with keratolimbal allograft transplantation using in vivo laser scanning confocal microscopy: an observational study. *Graefes Arch Clin Exp Ophthalmol.* 2011;249:701–708.
8. Shortt AJ, Secker GA, Munro PM, Khaw PT, Tuft SJ, Daniels JT. Characterization of the limbal epithelial stem cell niche: novel imaging techniques permit in vivo observation and targeted biopsy of limbal epithelial stem cells. *Stem Cells.* 2007;25:1402–1409.
9. Zheng T, Xu J. Age-related changes of human limbus on in vivo confocal microscopy. *Cornea.* 2008;27:782–786.
10. Baradaran-Rafii A, Javadi MA, Rezaei KM, Eslani M, Jamali H, Karimian F. Limbal stem cell deficiency in chronic and delayed-onset mustard gas keratopathy. *Ophthalmology.* 2010;117:246–252.
11. Baradaran-Rafii A, Eslani M, Tseng SC. Sulfur mustard-induced ocular surface disorders. *Ocul Surf.* 2011;9:163–178.
12. Ditta LC, Shildkrot Y, Wilson MW. Outcomes in 15 patients with conjunctival melanoma treated with adjuvant topical mitomycin c: complications and recurrences. *Ophthalmology.* 2011;118(9):1754–1759. [Epub 2011 Jun 8.]
13. Dua HS, Zuara-Blanco A. Limbal stem cells of the corneal epithelium. *Surv Ophthalmol.* 2000;44:415–425.
14. Fatima A, Iftekhar G, Sangwan VS, Vemuganti GK. Ocular surface changes in limbal stem cell deficiency caused by chemical injury: a histologic study of excised pannus from recipients of cultured corneal epithelium. *Eye (Lond).* 2008;22:1161–1167.
15. Hatch KM, Dana R. The structure and function of the limbal stem cell and the disease states associated with limbal stem cell deficiency. *Int Ophthalmol Clin.* 2009;49:43–52.
16. Javadi MA, Jafarinasab MR, Feizi S, Karimian F, Negahban K. Management of mustard gas-induced limbal stem cell deficiency and keratitis. *Ophthalmology.* 2011;118:1272–1281.
17. Kadar T, Dachir S, Cohen L, et al. Ocular injuries following sulfur mustard exposure—pathological mechanism and potential therapy. *Toxicology.* 2009;263:59–69.
18. Russell HC, Chadha V, Lockington D, Kemp EG. Topical mitomycin C chemotherapy in the management of ocular surface neoplasia: a 10-year review of treatment outcomes and complications. *Br J Ophthalmol.* 2010;94:1316–1321.
19. Tseng SC. Concept and application of limbal stem cells. *Eye (Lond).* 1989;3(pt 2):141–157.
20. Pellegrini G, Rama P, Mavilio F, De Luca M. Epithelial stem cells in corneal regeneration and epidermal gene therapy. *J Pathol.* 2009;217:217–228.
21. Patel DV, Sherwin T, McGhee CN. Laser scanning in vivo confocal microscopy of the normal human corneoscleral limbus. *Invest Ophthalmol Vis Sci.* 2006;47:2823–2827.
22. Srinivasan VJ, Wojtkowski M, Witkin AJ, et al. High-definition and 3-dimensional imaging of macular pathologies with high-speed ultrahigh-resolution optical coherence tomography. *Ophthalmology.* 2006;113:2054–2014.
23. Preibisch S, Saalfeld S, Tomancak P. Globally optimal stitching of tiled 3D microscopic image acquisitions. *Bioinformatics.* 2009;25:1463–1465.
24. Schmid B, Schindelin J, Cardona A, Longair M, Heisenberg M. A high-level 3D visualization API for Java and ImageJ. *BMC Bioinformatics.* 2010;11:274.
25. Ishikawa H, Kim J, Friberg TR, et al. Three-dimensional optical coherence tomography (3D-OCT) image enhancement with segmentation-free contour modeling C-mode. *Invest Ophthalmol Vis Sci.* 2009;50:1344–1349.
26. Gabriele ML, Wollstein G, Ishikawa H, et al. Optical coherence tomography: history, current status, and laboratory work. *Invest Ophthalmol Vis Sci.* 2011;52:2425–2436.
27. Bizheva K, Hutchings N, Sorbara L, Moayed AA, Simpson T. In vivo volumetric imaging of the human corneo-scleral limbus with spectral domain OCT. *Biomed Opt Express.* 2011;2:1794–1802.
28. Feng Y, Simpson TL. Comparison of human central cornea and limbus in vivo using optical coherence tomography. *Optom Vis Sci.* 2005;82:416–419.
29. Dua HS, Shanmuganathan VA, Powell-Richards AO, Tighe PJ, Joseph A. Limbal epithelial crypts: a novel anatomical structure and a putative limbal stem cell niche. *Br J Ophthalmol.* 2005;89:529–532.